Vibration mode frequency formulae for micromechanical scanners

2005 J. Micromech. Microeng. 15 1713

(http://iopscience.iop.org/0960-1317/15/9/013)

INSTITUTE OF PHYSICS PUBLISHING JOURNAL OF MICROMECHANICS AND MICROENGINEERING

J. Micromech. Microeng. **15** (2005) 1713–1721 doi:10.1088/0960-1317/15/9/013

Vibration mode frequency formulae for micromechanical scanners

Hakan Urey[1], **Cihan Kan**[2] **and Wyatt O Davis**[3]

[1] Electrical Engineering and Optical Microsystems Laboratory, Koç University, Istanbul, Turkey
[2] Turkish Airlines Maintenance Center, Yeşilköy, Istanbul
[3] Microvision Inc., Washington, USA

E-mail: hurey@ku.edu.tr

Received 8 December 2004, in final form 18 May 2005
Published 21 July 2005
Online at stacks.iop.org/JMM/15/1713

Abstract

A torsional scan mirror suspended with two flexure beams can be used in various display, imaging and other scanning applications. Using various mirror shapes and flexure dimensions as parameters, a set of analytical formulae is presented to predict the natural frequency of the first five vibration modes, which are torsion, in-plane and out-of-plane sliding modes and in-plane and out-of-plane rocking modes. Mode frequencies are compared with the finite element model (FEM) predictions using ANSYS™ for a wide range of flexure beam dimensions. The formulae include the effective inertia of the flexure beams and orthotropic material anisotropy effects. The analytical formulae are verified for both isotropic (e.g. steel) and orthotropic (e.g. silicon) materials. These formulae work very well when the Euler–Bernoulli beam theory assumptions and the rigid mirror assumption are satisfied. The accuracy of analytical predictions is improved by introducing an empirical correction factor to the analytical predictions using non-dimensional flexure beam ratios. The correction factor reduces the error between analytical formulae and FEM predictions to within a few per cent for all five modes for a large range of flexure dimensions. FEM predictions and analytical formulae are partly verified by experimental results.

(Some figures in this article are in colour only in the electronic version)

1. Introduction

Micro-optical scanners play an important role in scanned beam display [1] and imaging systems [2], and in MEMS optical cross-connects [3]. A two-axis gimbal mounted torsional scanner can create a raster pattern for display and imaging applications.

Basic one-axis torsional scanner geometry and the first five fundamental vibration modes are illustrated in figure 1. The two-axis scanner can be obtained by nesting two scan frames, one inside the other. There are several performance metrics for the scan mirror [4, 5]. System resolution requirements determine the mirror size and scan angle, the dynamic surface flatness requirements determine the mirror thickness and shape and mirror vibration frequency requirements determine the flexure beam dimensions that suspend the mirror [1, 6]. Thus, predicting the frequencies for the torsion and other fundamental vibration modes is critical. If the torsion is the desired mode, other modes are often undesired and should be well separated from the torsional mode frequency and its harmonics. As an example, in some applications, torsion and out-of-plane rocking mode should have a certain mode separation for simultaneous excitation [7]. Finite element model (FEM) simulations are time consuming, and engineering of the vibration mode frequencies for the optimal design is difficult without having good analytical models for fast calculations.

In this paper, we derive a compact set of formulae for making accurate predictions of the frequencies of the first five modes of a common class of microscanners, depicted in figure 1. The elements that comprise the formulae include expressions for the spring constants, effective inertias and correction factors for cases where the geometry does not motivate the theories used to derive the formulae. Some of

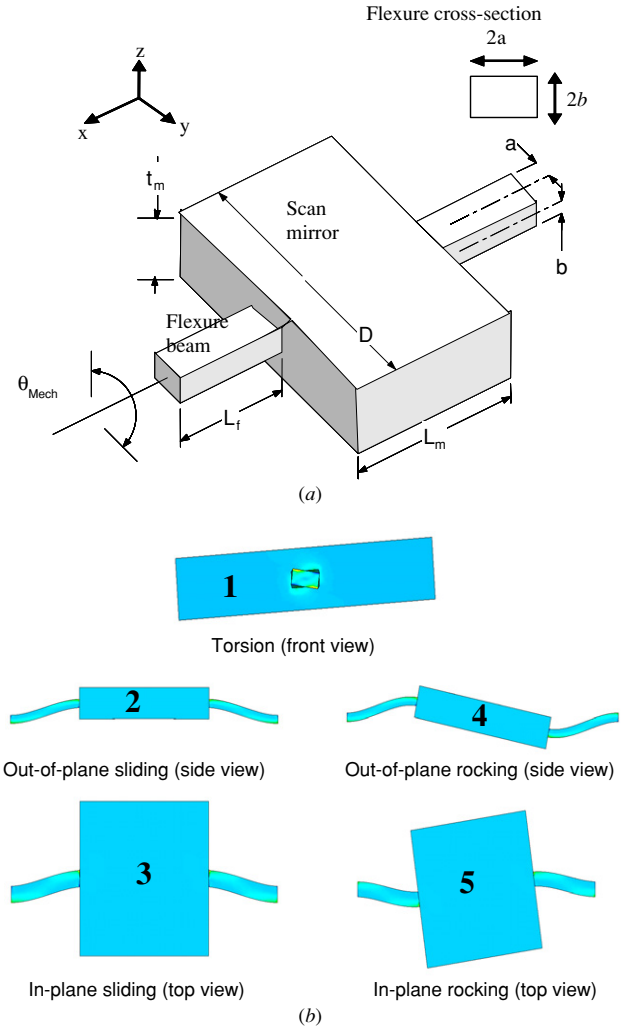

Figure 1. (*a*) Torsional resonant scan mirror suspended with two flexure beams that are fixed at the ends; the inset shows the flexure rectangular cross-section and coordinate axis. (*b*) Five fundamental vibration modes for the torsional scanner, which are rotation around the *x*-axis (torsional), translation in the *z*-axis (out-of-plane translation), translation in the *y*-axis (in-plane sliding), rotation around the *y*-axis (out-of-plane rocking) and rotation around the *z*-axis (in-plane rocking).

these elements can be found elsewhere, including expressions for some of the spring constants and treatments of Rayleigh's method for computing effective inertias. The unique features of this paper are a concise tabulation of spring constant and inertia formulae for the five most important modes of a common MEMS design, the inclusion of material orthotropy in the calculation of torsion spring constant, development of dimensionless parameters for parametric design of similar structures and the development of an analytical/graphical method for adjusting the formulae to correct known modeling errors.

Section 2 presents the derivations of formulae for the spring constants and effective inertias for the five modes of interest. The spring constants include the effects of orthotropic material properties for torsion. Even though single-crystal silicon is orthotropic, isotropic torsion frequency formulae that are found in [8] are used in several papers in the MEMS literature [9–13], which leads to unnecessary errors. Our formulae for torsion can handle orthotropic materials and improve the frequency predictions.

Mode frequency predictions are improved by modeling the effective mass and inertia of the beam, which are calculated using Raleigh's method [14]. The formulae for the effective inertias for several typical cases, including rectangular and elliptical mirror shapes, are provided. Section 3 summarizes the results of section 2 in a table format.

In section 4, a parametric study is performed comparing formulae with FEM results using two dimensionless parameters based on flexure dimensions and fixed torsion frequency. The material modeling is discussed for silicon and steel in the analytical formulae and in FEM software. Results of the parametric analysis are used to calculate error charts. These errors are induced when certain non-dimensional ratios tend toward extreme values, where the assumptions underlying the Euler–Bernoulli beam model for bending and Saint Venant uniform torsion model break down. In this section, we discuss the application of correction factors derived from the error charts to extend the applicability of the formulae while maintaining their simplicity.

2. Analytical formulae for spring constant

Figure 1(*a*) illustrates a rectangular-block torsional microscanner. The first six fundamental vibration modes are the translational and rotational oscillations along or around the *x*-, *y*- and *z*-axes. In this section, the spring stiffnesses for five modes are derived. Translation along *x* is not treated as the beam is fixed at two ends, and typically the axial stiffness is so high that modes involving deformations of the mirror plate will occur at lower frequencies than the *x*-translation mode. Figure 1(*b*) illustrates the five fundamental vibration modes that we refer to as the torsional mode, out-of-plane and in-plane sliding modes and out-of-plane and in-plane rocking modes. We use the orthogonality of the modal coordinates to model the microscanner as a one degree-of-freedom system with lumped mass approximation. One can calculate the natural frequencies of each vibration mode by using appropriate displacement or rotation angle variable, spring constant and effective mass or effective mass moment of inertia terms. As an example, the natural frequency for the vibration mode along the *y*-axis (in-plane sliding) with angular frequency ($\omega = 2\pi f$) can be calculated by [15]

$$\frac{\mathrm{d}^2 y}{\mathrm{d}t^2} + \omega^2 y = 0 \tag{1}$$

$$\omega = 2\pi f = \sqrt{K_s / M_{\mathrm{eff}}} \tag{2}$$

where K_s is the spring constant for the mode and M_{eff} is the effective mass of the scan mirror for the particular vibration mode. Throughout our analysis, the mirror plate is assumed rigid and flexures are assumed fixed on either end. In addition, damping is ignored in (1) because of the typically negligible effect on the natural frequency for underdamped systems.

2.1. Torsion mode

The derivation of torsional stiffness is obtained using the Saint Venant theory of uniform torsion ([16], chapter 11). This

method estimates torsional spring constant as a product of torsional modulus (G) and torsional stiffness (K) (GK-product) and inversely proportional to the flexure length (L_f). The solution is valid for isotropic materials (e.g. steel) and for materials where the compliance or stiffness matrix shows at least orthotropic anisotropy in global coordinates (e.g. single-crystal silicon) [17, 18]. If a net torque T is applied to the mirror around the x-axis, then the following angular momentum balance can be used (by taking $T = 0$) to compute the natural frequency of the torsional mode for small rotation angles:

$$J_{\mathrm{m},xx}\frac{\mathrm{d}^2\theta_\mathrm{mech}}{\mathrm{d}t^2} + \frac{2(GK)\theta_\mathrm{mech}}{L_\mathrm{f}} = T \tag{3}$$

where θ_mech is the mechanical rotation angle, and $J_{\mathrm{m},xx}$ is the lumped moment of inertia of the system. The GK-product depends on the shape of flexure cross-section and the linear anisotropic material coefficients evaluated in the global Cartesian coordinate system. If the solution given in [8] for isotropic materials is expanded for an orthotropic medium, the GK-product for rectangular flexures can be calculated as

$$GK = \frac{2^{12}ab}{\pi^6}\sum_{\substack{n=1\\ \mathrm{odd}}}^{\infty}\sum_{\substack{m=1\\ \mathrm{odd}}}^{\infty}\frac{1}{m^2n^2}\left(\frac{m^2}{a^2G_{xz}} + \frac{n^2}{b^2G_{xy}}\right)^{-1}. \tag{4a}$$

After some algebra, 4a can be reduced to a single summation that converges faster:

$$GK = \left(\frac{16}{3}ab^3G_{xy}\right)\left(1 - \frac{192}{\pi^5\mu}\left(\frac{b}{a}\right)\right.$$
$$\left.\times\left\{\sum_{\substack{n=1,3\\ (\mathrm{odd})}}^{\infty}\left(\frac{1}{n^5}\tanh\left[\frac{n\pi\mu a}{2b}\right]\right)\right\}\right) \tag{4b}$$

where $\mu = \sqrt{G_{xz}/G_{xy}}$ is due to material anisotropy and is equal to 1 for isotropic materials. The series solution given above is rapidly converging. Using the analogy with the isotropic material formula given in [8], the following simple approximation is found:

$$GK \approx (ab^3G_{xy})\left(5.33 - 3.36\frac{b}{a}\frac{1}{\mu}\left(1 - \frac{b^4}{12a^4\mu^4}\right)\right). \tag{5}$$

Equations (4) and (5) are valid for $a\mu >$ b. If $b > a\mu$, then $a\mu$-*product* and b should be interchanged, and G_{xy} and G_{xz} should be interchanged in these equations. The above equation works well even for stubby flexures whose lengths are not large compared to a or b.

Even though single-crystal silicon is anisotropic, some of the MEMS literature use $\mu = 1$ in the above expressions for computing torsional stiffness for silicon [10–14]. Using the correct $\mu = 1.248$ for $\langle 1\,0\,0\rangle$ silicon in our new formula improves the accuracy of the torsional stiffness computation by as much as 20% in some cases.

2.2. Sliding and rocking modes

The sliding and rocking modes involve beam bending, which we model by using the Euler–Bernoulli beam theory. For these bending modes, the stiffness is derived by solving a fourth-order ODE for the deflection of the neutral axis, $w_0(x)$ [19]:

$$\frac{\mathrm{d}^4w_0(x)}{\mathrm{d}x^4} = 0 \tag{6}$$

where subscript '0' refers to the deflection curve of the neutral axis of the flexures. The boundary conditions are prescribed according to the particular mode being treated. The displacement at the end of the beam that is attached to the scanning mirror is taken to be consistent with the modal coordinate. The force and moment acting on the beam end are computed as

$$F = EI\left.\frac{\mathrm{d}^3w_0(x)}{\mathrm{d}x^4}\right|_{x=L_\mathrm{f}} \tag{7}$$

$$M = EI\left.\frac{\mathrm{d}^2w_0(x)}{\mathrm{d}x^2}\right|_{x=L_\mathrm{f}}. \tag{8}$$

The effective stiffness can be computed by taking an appropriate sum of the forces and moments on the beam-end and by applying a balance of translational or angular momentum for the scanning mirror.

2.3. Out-of-plane sliding mode

The boundary conditions are

$$\begin{aligned} w_0(0) &= 0, \quad & w_0'(0) &= 0,\\ w_0(L_\mathrm{f}) &= z, \quad & w_0'(L_\mathrm{f}) &= 0 \end{aligned} \tag{9}$$

where z is the out-of-plane displacement of the scanning mirror. The solution of the ODE for $w_0(x)$, F and M is omitted in the interest of brevity. The balance of translational momentum for the scanning mirror is

$$M_\mathrm{eff}\ddot{z} + K_\mathrm{s}z = F_z \tag{10}$$

where damping forces are ignored. For static solutions of (10), $\ddot{z} = 0$, and we obtain the spring constant K_s by considering the forces, computed using (7), acting on the scanning mirror due to the beam displacements:

$$K_\mathrm{s}z = F_z = -2F \tag{11}$$

which provides

$$K_\mathrm{s} = 24E_xI_{yy}/L_\mathrm{f}^3 \tag{12}$$

where E_x is Young's modulus in the x direction for an orthotropic material and $I_{yy} = 4ab^3/3$ is the second moment of inertia with respect to the y-axis for the flexure cross-sectional area.

The total mass is that of the scanning mirror and some inertia from the suspension beams. We can obtain the latter contribution to the mass using Raleigh's method, which is discussed in section 3 [14]:

$$M_\mathrm{eff} = M_\mathrm{m} + \frac{26}{35}M_\mathrm{f} \tag{13}$$

where M_m is the mirror mass and $M_\mathrm{f} = 4abL_\mathrm{f}$ is the mass of one flexure.

Now, knowing the parameters K_s and M_eff we can rewrite (10) (with $F_z = 0$) in the form of (1) and solve for the modal frequency. This step is omitted in the interest of brevity, but a discussion of the accuracy of the calculation is provided in a later section.

Table 1. Parameters used for computing the natural frequencies for five fundamental oscillation modes for torsional scanners. M_m and J_m are the mass and mass moment of inertia of the mirror (defined in table 2), and M_f is the mass of one flexure.

	Effective mass (M_eff) and effective mass moment of inertia (J_eff)	Spring constant (K_s)
1. Torsion	$J_\mathrm{eff} = J_{\mathrm{m},xx} + (2/3)J_{\mathrm{f},xx}$	$K_\mathrm{s} = \frac{2GK}{L_\mathrm{f}}$; $\mu = \sqrt{G_{xz}/G_{xy}}$, where GK is given by
	$J_{\mathrm{f},xx} = \frac{1}{3}M_\mathrm{f}(a^2+b^2)$	$GK = \begin{cases} (ab^3G_{xy})\left(5.33 - 3.36\frac{b}{a\mu}\left(1-\frac{b^4}{12a^4\mu^4}\right)\right) & a\mu \geqslant b \\ (ba^3G_{xz})\left(5.33 - 3.36\frac{a\mu}{b}\left(1-\frac{a^4\mu^4}{12b^4}\right)\right) & a\mu \leqslant b \end{cases}$
	$M_\mathrm{f} = 4abL_\mathrm{f}$	
2. Out-of-plane sliding	$M_\mathrm{eff} = M_\mathrm{m} + \frac{26}{35}M_\mathrm{f}$	$K_\mathrm{s} = \frac{24E_xI_{yy}}{L_\mathrm{f}^3}$; $I_{yy} = \frac{4}{3}ab^3$
3. In-plane sliding	$M_\mathrm{eff} = M_\mathrm{m} + \frac{26}{35}M_\mathrm{f}$	$K_\mathrm{s} = \frac{24E_xI_{zz}}{L_\mathrm{f}^3}$; $I_{zz} = \frac{4}{3}a^3b$
4. Out-of-plane rocking	$J_\mathrm{eff} = J_{\mathrm{m},yy} + 2J_\mathrm{f}$ $J_\mathrm{f} = M_\mathrm{f}(0.0095L_\mathrm{f}^2$ $+0.052L_\mathrm{f}L_\mathrm{m} + 0.0929L_\mathrm{m}^2)$	$K_\mathrm{s} = \frac{E_xI_{yy}\left(2+6\left(1+\frac{L_\mathrm{m}}{L_\mathrm{f}}\right)^2\right)}{L_\mathrm{f}}$
5. In-plane rocking	$J_\mathrm{eff} = J_{\mathrm{m},zz} + 2J_\mathrm{f}$	$K_\mathrm{s} = \frac{E_xI_{zz}\left(2+6\left(1+\frac{L_\mathrm{m}}{L_\mathrm{f}}\right)^2\right)}{L_\mathrm{f}}$

Table 2. Mass and mass moment of inertia for different mirror shapes.

	M_m	$J_{\mathrm{m},xx}$	$J_{\mathrm{m},yy}$	$J_{\mathrm{m},zz}$
Rectangular mirror	$\rho L_\mathrm{m}Dt_\mathrm{m}$	$\frac{M_\mathrm{m}}{12}\left(D^2+t_\mathrm{m}^2\right)$	$\frac{M_\mathrm{m}}{12}\left(L_\mathrm{m}^2+t_\mathrm{m}^2\right)$	$\frac{M_\mathrm{m}}{12}\left(D^2+L_\mathrm{m}^2\right)$
Elliptical mirror	$\frac{\pi}{4}\rho L_\mathrm{m}Dt_\mathrm{m}$	$\frac{M_\mathrm{m}}{12}\left(\frac{3}{4}D^2+t_\mathrm{m}^2\right)$	$\frac{M_\mathrm{m}}{12}\left(\frac{3}{4}L_\mathrm{m}^2+t_\mathrm{m}^2\right)$	$\frac{M_\mathrm{m}}{16}\left(D^2+L_\mathrm{m}^2\right)$
Circular mirror	$\frac{\pi}{4}\rho D^2t_\mathrm{m}$	$\frac{M_\mathrm{m}}{12}\left(\frac{3}{4}D^2+t_\mathrm{m}^2\right)$	$\frac{M_\mathrm{m}}{12}\left(\frac{3}{4}D^2+t_\mathrm{m}^2\right)$	$\frac{M_\mathrm{m}}{8}(D^2)$

2.4. In-plane sliding mode

The mode moves the mirror along the y-axis and formulae are similar to out-of-plane sliding formulae. Interchanging the flexure width (a) with flexure thickness (b) and replacing I_{yy} with I_{zz} in the above formulae is sufficient. For square cross-section flexures, as long as the bending in the mirror is negligible, the horizontal and vertical mode frequencies are identical.

2.5. Out-of-plane rocking mode

The boundary conditions for the ODE are

$$\begin{aligned} w_0(0) &= 0; \qquad & w_0'(0) &= 0; \\ w_0(L_\mathrm{f}) &= L_\mathrm{m}\theta_\mathrm{m}/2; \qquad & w_0'(L_\mathrm{f}) &= -\theta_\mathrm{m}. \end{aligned} \tag{14}$$

The balance of angular momentum for the scanning mirror is

$$J_{\mathrm{m},yy}\frac{\mathrm{d}^2\theta_\mathrm{m}}{\mathrm{d}t^2} + K_\mathrm{s}\theta_\mathrm{m} = T. \tag{15}$$

Recognizing that ([8], table 8.17, cases 1a–3a)

$$T = -2(M + FL_\mathrm{m}). \tag{16}$$

The beam deflection can be solved in terms of rotation of mirror θ_m.

$$w_0(x) = \frac{-\theta_\mathrm{m}(L_\mathrm{f}+L_\mathrm{m})}{L_\mathrm{f}^3}x^3 + \frac{\theta_\mathrm{m}(L_\mathrm{f}+1.5L_\mathrm{m})}{L_\mathrm{f}^2}x^2. \tag{17}$$

Using (7) and (8) with the static solution of the momentum balance (15) provides the spring constant

$$K_\mathrm{s} = \frac{-T}{\theta_\mathrm{m}} = \left[\left(6\left(\frac{L_\mathrm{m}}{L_\mathrm{f}}\right)^2 + 12\frac{L_\mathrm{m}}{L_\mathrm{f}} + 8\right)\frac{E_xI_{yy}}{L_\mathrm{f}}\right]. \tag{18}$$

2.6. In-plane rocking mode

These formulae are similar to above and can be obtained by substituting E_xI_{zz} by E_xI_{yy} and by calculating the mirror mass moment of inertia around the z-axis. For the geometries considered, the in-plane rocking mode frequency is typically higher than the out-of-plane rocking mode frequency.

2.7. Analytical formulae for beam effective inertia

Effective inertia of the flexure beam is calculated below for the out-of-plane rocking mode. Derivations for other modes are simpler and the results are summarized in table 1.

Using (17), we can express the single flexure beam velocity and kinetic energy stored as follows:

$$\frac{\mathrm{d}w_0(x)}{\mathrm{d}t} = \frac{\mathrm{d}\theta_\mathrm{m}}{\mathrm{d}t}\left(\frac{-(L_\mathrm{f}+L_\mathrm{m})}{L_\mathrm{f}^3}x^3 + \frac{(L_\mathrm{f}+1.5L_\mathrm{m})}{L_\mathrm{f}^2}x^2\right) \tag{19}$$

$$\begin{aligned} \mathrm{KE_f} &= \int_0^{L_\mathrm{f}}\frac{1}{2}(4\rho ab)\left(\frac{\mathrm{d}w_0(x)}{\mathrm{d}t}\right)^2\mathrm{d}x \\ &= \frac{M_\mathrm{f}}{2}\left(0.0095L_\mathrm{f}^2 + 0.052L_\mathrm{f}L_\mathrm{m} + 0.093L_\mathrm{m}^2\right) \\ &\quad\times\left(\frac{\mathrm{d}w_0(L_\mathrm{f})}{\mathrm{d}t}\right)^2. \end{aligned} \tag{20}$$

The mirror kinetic energy and the total kinetic energy of the system are then given by

$$\mathrm{KE_m} = \frac{1}{2}J_{\mathrm{m},yy}\left(\frac{\mathrm{d}\theta_\mathrm{m}}{\mathrm{d}t}\right)^2 \qquad \mathrm{KE_{total}} = \mathrm{KE_m} + 2\mathrm{KE_f}. \tag{21}$$

An effective inertia can be defined using relative contributions of the flexures and the mirror:

$$J_{\text{eff}} = 2J_{\text{f}} + J_{\text{m},yy}$$
$$J_{\text{f}} = M_{\text{f}}\left(0.0095L_{\text{f}}^2 + 0.052L_{\text{f}}L_{\text{m}} + 0.093L_{\text{m}}^2\right). \quad (22)$$

Note that for torsion mode, the flexure inertia is less than a few per cent of the mirror inertia and often negligible. For sliding modes, the flexure mass should be included in the calculation for long and wide flexures. For rocking modes, the flexure inertia can be larger than the mirror inertia and should definitely be included in the effective inertia calculations.

3. Summary of analytical results

Table 1 summarizes the spring constant, effective inertia including the flexure-inertia terms for five fundamental modes. The formulae for the spring constants are consistent with values given elsewhere in the literature [20, 21]. Table 2 gives mirror inertia for different mirror shapes. The natural frequency of a mode can be calculated using (2). The formulae in tables 1 and 2 can be used to predict the mode frequencies, which give important information about the sequence of different modes and the relative frequency separation between modes. Once a good design point is reached using the analytical calculations, FEM simulations should be used for more accurate predictions using the exact mirror geometry.

Because of the assumptions inherent to the Euler–Bernoulli beam theory, the derivations above are applicable to slender beams with sufficiently low vibration frequencies. The sliding and rocking mode analytical frequency formulae presented in table 2 can be improved using the Timoshenko beam theory that takes into account two effects neglected in the Euler–Bernoulli theory: rotary inertia and shear deformation effects [21–29]. The resulting formulae will be somewhat less compact and still require error correction terms for high-aspect ratio beams. In this paper, we emphasize simplicity in the formulae. In the sections that follow, we will examine corrections that may be applied to the formulae to handle this known modeling error for non-slender beams.

An important assumption in our analysis is that all deformations take place at the flexures, i.e. the mirror is rigid. This assumption is generally valid except for the cases when the mirror to flexure width ratio ($D/2a$) is about unity and the mirror thickness is too small compared to width and length of the mirror. For typical optical applications, the mirror surface must remain flat to within 20–50 nm for keeping the aberrations under control; thus the mirror is already constrained to be chosen thick enough to avoid bending of the mirror during operation due to large acceleration forces [4].

Note that these mode frequency formulae are valid for rectangular, circular and elliptical block mirrors with flexures that have rectangular cross-section. Other flexure and mirror shapes and shifts in the axis of rotation can also be analyzed by substituting appropriate values of mass and inertia for the mirror and the flexures in the corresponding formulae. All of the spring constants are derived for orthotropic materials, and proper simplifications are made to find the results for silicon and steel as exemplary scanner materials.

4. Validity range of analytical formulae

We first tested the validity of our analytical formulae using a steel rectangular-box scanner design with the following mirror and flexure dimensions (all in microns):

A	b	L_{f}	D	L_{m}	t_{m}
40	40	1000	1500	1500	300

The following analytical and FEM predictions were obtained for the first five modes (as numbered in figure 1):

Modes	1	2	3	4	5
Analytical (f_{a}) (Hz)	4723	8913	8913	25 619	18 600
FEM (f_{fem}) (Hz)	4707	8603	8631	24 625	17 905
% Error	−0.35	−3.6	−3.27	−4.04	−3.87

where the error is defined as

$$\%\,\text{error} = 100\left[\frac{f_{\text{fem}} - f_{\text{a}}}{f_{\text{a}}}\right]. \quad (23)$$

Note that analytical and FEM predictions using ANSYS are within 4% of each other for all modes. When the rigid mirror assumption is imposed on FEM computations by making the mirror piece artificially stiffer, the maximum error reduces to 0.5%. The test case validates our analytical formulae given in tables 1 and 2.

A case that is more attractive for us is a scanner operating around 20 kHz as it can be used in SVGA (800 × 600) resolution retinal scanning display system [1]. Next we describe how material properties are modeled in ANSYS for steel and silicon, and then discuss the results of parametric study for 15 different scanner designs, which has the same mirror dimensions and torsion frequency but different flexure dimensions.

4.1. Material properties and FEM modeling

Elastic properties of steel are independent of direction and contain only two independent coefficients: modulus of elasticity E and Poisson ratio ν, whereas silicon as a cubic material has the simplest material anisotropy with three different material constants at its principal material Cartesian coordinate system [30]. When the coordinate system used for describing nodal degrees of freedom does not coincide with the principal material coordinate system of silicon, the material matrix coefficients have to be changed to align with the nodal coordinate system [31]. The new material matrix usually contains more than three coefficients [32]. The solution coordinate system used for FEM calculations for silicon structures fabricated from (1 0 0) wafers is obtained by a rotation of principal material Cartesian coordinate system of 45° around the ⟨1 0 0⟩ direction, or z-axis. The material properties of steel and silicon (in the solution coordinate system) used in the analytical formulae are given in table 3.

Classical formulae used to calculate vibration characteristics of isotropic structures are not applicable to single crystal ⟨1 0 0⟩ silicon microscanners unless the effect

Table 3. Engineering material coefficients for steel and silicon in global coordinates. E and G are in Pa.

	Steel	Silicon
E_x	2.03×10^{11}	1.7×10^{11}
E_y	2.03×10^{11}	1.7×10^{11}
E_z	2.03×10^{11}	1.30×10^{11}
ν_{xy}	0.293	0.064
ν_{xz}	0.293	0.36
ν_{yz}	0.293	0.36
G_{xy}	7.85×10^{10}	5.1×10^{10}
G_{xz}	7.85×10^{10}	7.94×10^{10}
G_{yz}	7.85×10^{10}	7.94×10^{10}

of the crystal orientation is taken into account. The material constants in table 3 can be used in the formulae in table 1 when the flexure axes correspond to a $\langle 1\,1\,0 \rangle$ direction. A detailed description of how to calculate rotated material constants of cubic materials is given in [30] and [33].

An APDL programming language-based ANSYS macro is created for easy and quick FEM calculations. The calculations are carried out for constant mirror dimensions and the flexure geometry is arranged according to analytical formulae to get the torsional frequency at about 20 kHz. All of the nonlinear and transient effects are neglected in the FEM model and linear vibration analysis carried out with block Lanczos solution control.

4.2. Parametric study of flexure dimensions

Using three flexure dimensions and imposing a constraint on the torsion frequency, we can define two dimensionless flexure parameters k and n. The k parameter is equal to ratio of height to width ratio of rectangular cross-section (i.e., $k = a/b$). The n parameter is the ratio of the beam length L_f to the larger of the two sides of the rectangular beam cross-section.

Cases where $a > b$ (wide flexure beams) are mostly encountered in high-frequency bulk micromachined microscanners [4]. Cases where $b > a$ are mostly encountered in surface micromachined and SOI bulk micromachined scanners operating at lower frequencies. Wafer thickness and flexure thickness are often equal in those cases [34].

The aim of the parametric study using dimensionless parameters is to make the results of error analysis applicable to other scanner designs that have the same flexure ratio parameters (k, n) but different mirror dimensions and torsion frequencies.

For our study, we fixed the torsion frequency to be near 20 kHz and used the following mirror dimensions in the analytical and FEM calculations using ANSYS^{TM}:

$$D_m = 1.5 \text{ mm}; \qquad L_m = 1.5 \text{ mm}; \qquad t_m = 0.3 \text{ mm}. \tag{24}$$

We studied both silicon and steel as microscanner materials and tested 15 different (k, n) combinations for flexure width ratio values of $k = [1, 2, 3]$ and flexure length ratios of $n = [2, 4, 6, 8, 10]$, exploring a large portion of the flexure design space. The error is calculated using (23). As a design point reference, for different values of (k, n), flexure dimensions took on values in the following range:

	a (μm)	b (μm)	L_f (μm)
Min	114	92	227
Max	473	194	4732

When $b > a$, we defined two new parameters $k_2 = b/a$ and $n_2 = L_f/2b$. We compare the predictions of the analytical formulae with FEM results for a number of test cases.

4.3. Discussion on validity range of formulae

Figures 2 and 3 summarize the results of our parametric study, comparing our analytical results with FEM simulations. There are several observations that can be made using the graphs in figure 2. First, error predictions are very similar for steel and silicon. Thus, the comments that follow are applicable to both materials.

Torsion frequency predictions are always within 10% even for wide and short flexures (large k, small n) and within 3% for $n > 4$. We separately tested the contribution of the flexure inertia term and it is not negligible especially for large values of n.

Formulae predict the other four vibration mode frequencies to within ~10% for $n > 6$. Including the effects of flexure effective mass and flexure effective mass moment of inertia become particularly important for long flexures ($n > 6$). Error for non-torsion modes is always negative (i.e., formulae over-predict the vibration frequencies). Our model includes constraints on the shear deformations within the suspension and on the deformation of the mirror. Neglecting these deformations causes an over prediction of the stiffness, i.e. the actual spring constant and the frequency are lower than the formula predictions. The effect of shear deformations (ignored in the Euler–Bernoulli beam theory) becomes particularly significant for small flexure length ratios n. Likewise, this is apparent from the plots in figures 2(b) and (d): when k is increased for a given n, L_f/b ratio increases, reducing the error for the out-of-plane modes.

The percentage errors corresponding to translation and rocking modes are very similar for both in-plane and out-of-plane modes. This is expected due to the same physics and dimensions in the bending direction.

Figure 3 illustrates the error predictions for a number of cases where $a = b$, $a > b$ and $b > a$ as a function of (k, n) and (k_2, n_2) values as defined in the figure. Observations for $b > a$ cases are similar to those for $a > b$, which was illustrated in figure 2(d). For torsion mode, the errors for same (k, n) = (k_2, n_2) pairs are about the same (e.g. compare cases where $(k, n) = (k_2, n_2) = (2, 6)$. For isotropic materials, the errors in each case should be identical, for anisotropic silicon, some difference is anticipated due to differences in G_{xy} and G_{xz}, but the torsion mode errors turn out to be about the same. For sliding and rocking modes, however, the error predictions for in-plane modes for a (k, n) pair become the error prediction for the out-of-plane mode for the same (k_2, n_2) pair, and vice versa. The difference, if any, is mainly due to bending of the mirror plate in out-of-plane modes.

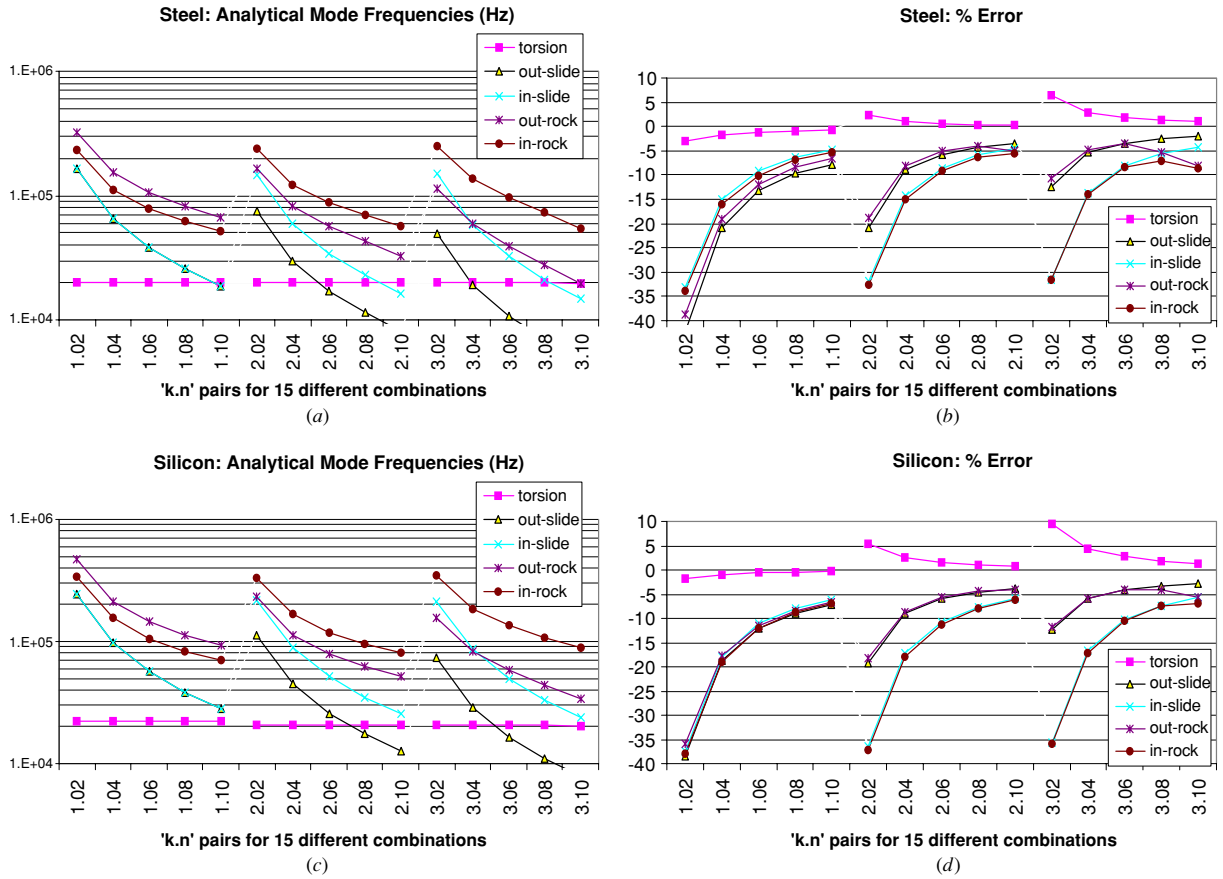

Figure 2. Mode frequency calculations using analytical formulae and percentage error compared to FEM for 15 different microscanner designs (horizontal axes shows k.n pairs, e.g. 2.04 means $k = 2$, $n = 4$). All microscanners have approximately 20 kHz torsion frequency but different flexure dimensions as determined by (k, n) pairs. (*a*) Mode frequencies for steel (example of isotropic material), (*b*) % error for steel, (*c*) mode frequencies for silicon (cubic material), (*d*) % error for silicon.

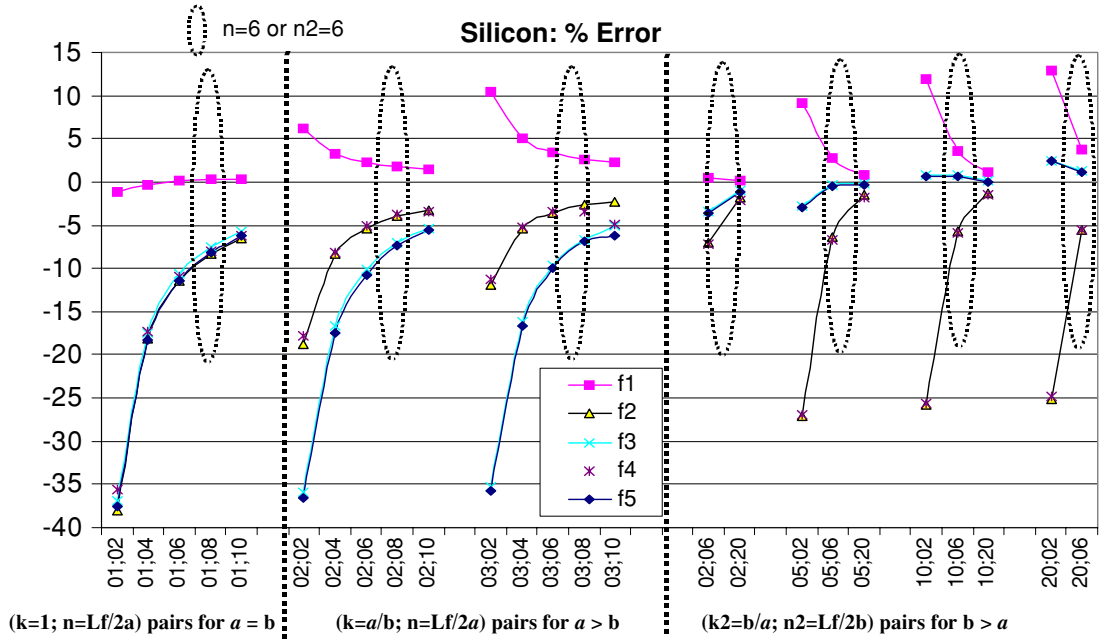

Figure 3. Percentage error between analytical formulae in table 2 and FEM calculations using ANSYS™ for a number of microscanner designs. The results are reported based on $(k; n)$ and $(k_2; n_2)$ values as defined in the horizontal axis label.

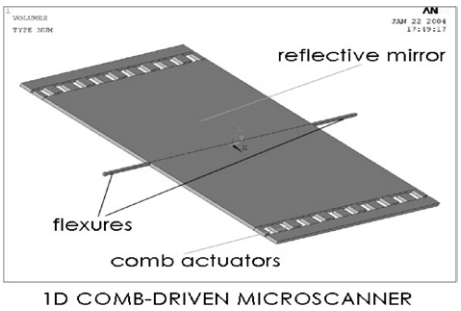

Figure 4. Comb-driven microscanner produced by Fraunhofer IPMS, Germany [34, 35].

Table 4. Error comparison for microscanner designs at different frequencies. Rows 1–3, rows 5–6 and rows 7–8 have same (n, k) values but different design frequencies.

			% Error for five modes				
K	n	f_1 (Hz)	1	2	3	4	5
1	8	22 027	−0.4	−8.9	−8.0	−8.6	−8.8
1	8	1000	−0.7	−6.5	−7.2	−6.7	−7.4
1	8	5 000	−0.8	−6.9	−7.7	−7.2	−8.2
2	2	20 876	5.5	−19.4	−36.3	−18.3	−37.0
2	2	1000	5.7	−14.6	−35.2	−14.5	−35.3
2	5	1000	2.1	−4.4	−11.6	−4.5	−11.9
2	5	5 000	1.6	−5.8	−12.7	−6.1	−13.4

4.4. Correction factors for the formulae

Since the results are obtained using dimensionless flexure parameters, one can try a different set of values for flexure dimensions and mirror dimensions and then add the error corresponding (k, n) pair in their design as an additional correction factor to the analytical formulae. If a, b and L_f are known for a design, the data points in the error charts in figures 2 and 3 can be interpolated to find an appropriate correction factor.

With the correction factors, one can obtain accurate mode frequency predictions for beam dimensions where the Euler–Bernoulli theory normally fails.

To further support this claim, we designed a set of microscanners with different frequencies but the same (k, n) pairs. As listed in table 4, the error between formula and FEM results is about the same for a given (k, n) pair independent of the frequency. Therefore, the correction factors, determined from figures 2(b), (d) or 3 can be applied to any microscanner design, greatly enhancing the validity range of analytical formulae presented in table 1.

4.5. Experimental results

We tested a number of torsional scanners and validated analytical formulae. Torsion mode formula predictions are within a few per cent of the FEM and experimental predictions. Comb-driven microscanner seen in figure 4 is a rectangular box-shaped microscanner. The mirror inertia is computed by adding the mirror plate inertia and comb finger inertia terms, which is calculated by proper weighting of the material density with the fill factor of the combs. Table 5 compares torsion mode analytical and experimental results. Torsion mode predictions for various scanners are all within 10%.

Table 5. Experimental results for three different microscanners.

Scanner model number	SL28	E201-30	CB02
Mirror shape	Round	Square	Round
Flexure width ratio, $k = a/b$	1/16	2.1	1.9
Flexure length ratio, n	6.7	19.6	6.2
Torsion_formula (Hz)	251	1168	7985
Torsion_experimental (Hz)	270	1069	8450
Torsion ANSYS (Hz)	250		
Out-of-plane bending formula (Hz)	20 613		
Out-of-plane bending analytical with the correction factor using figure 3 (Hz)	19 376		
Out-of-plane bending ANSYS (with rigid mirror imposed)	19 385		
Out-of-plane bending experimental (Hz)	16 420		
Out-of-plane bending ANSYS (mirror can also bend)	17 809		

We tested the out-of-plane bending mode for model SL28 using a laser Doppler vibrometer (LDV). For SL28, the flexure length is 200 μm, the flexure thickness ($2b$) is 30 μm and the flexure width ($2a$) is only 1.8 μm. For this geometry $a\mu < b$ and the dimensionless parameters can be calculated as $k_2 = 16.7$ and $n_2 = 6.7$. The sliding mode error for this case was measured as −20%, worse than –6%, which is estimated from figure 3 using the closest data points (10; 6) and (20; 6) for (k_2, n_2) pairs. We suspect that the discrepancy between the analytical and the experimental results is due to the bending of the mirror plate, which is ignored in our analytical treatment. To prove this, we performed two FEM simulations: (1) where the mirror and flexures are both silicon, and (2) where a rigid mirror assumption is imposed to the mirror plate by using coupling equations technique. Note that in table 5, the error between the corrected formula and FEM is smaller than 1% (only 9 Hz) when the rigid mirror assumption is imposed, and the FEM result agrees well with the experimental result when mirror is silicon and allowed to bend. This case illustrates the utility of the error correction and the analytical formulae even for such extreme flexure width ratios. We cannot excite out-of-plane rocking mode for this scanner even under low damping vacuum conditions. Measuring in-plane modes is difficult in this structure due to the pull-in of comb fingers.

5. Conclusions

We presented analytical formulae that can be used to estimate the first five natural frequencies of flexure-mounted torsional mirrors for a broad range of flexure dimensions and various mirror shapes. Tables 1 and 2 give spring constant and inertia terms corresponding to the five fundamental oscillation modes for flexure-mounted scanner designs. Our formulae can handle orthotropic material properties and include effects of the flexure beam inertia. Using the beam-width-ratio parameter and the beam-length-ratio parameter for a scanner design, a correction factor based on error charts in figures 2 and 3 can be added to the analytical formulae to improve the accuracy of the predictions. Using the correction factors, the analytical formulae become accurate to within a few per cent of FEM predictions in all cases for a broad range of flexure

dimensions, including ranges where assumptions underlying the Euler–Bernoulli beam theory do not hold.

The work presented in all sections point to the efficiency of the analytical formulae presented in the paper. For conceptual design studies these formulae may be used for the first dimensioning purposes at early design steps to assure good mode separation and low stress on the beam. The final verification should be based on detailed FEM modeling of the structure.

Acknowledgments

We thank Microvision for sponsoring this research, Fraunhofer IPMS for providing microscanners for testing and Dean Brown and Caglar Ataman for help with ANSYS simulations and experimental results.

References

[1] Urey H 2003 Retinal scanning displays *Encyclopedia of Optical Engineering* vol 3 ed R Driggers (New York: Dekker) pp 2445–57

[2] Dickensheets D L and Kino G S 1998 Silicon micromachined scanning confocal optical microscope *J. Microelectromech. Syst.* **7** 38–47

[3] Lin L Y and Goldstein E L 2002 Opportunities and challenges for MEMS in lightwave communications *J. Sel. Top. Quantum Electron.* **8** 163–72

[4] Urey H, Wine D W and Osborn T D 2000 Optical performance requirements for MEMS-scanner based microdisplays *Proc. SPIE* **4178** 176–85

[5] Urey H 2004 Spot size, depth of focus, and diffraction ring intensity formulas for truncated Gaussian beams *Appl. Opt.* **43**

[6] Urey H, Wine D W and Lewis J R 1999 Scanner design and resolution tradeoffs for miniature scanning displays *Proc. SPIE* **3636** 60–8

[7] Garnier A, Bourouina T, Orsier E, Masuzawa T, Fujita H, Hiramoto T and Peuzin J-C 2000 A fast simple and robust 2-D micro-optical scanner based on contactless magnetostrictive actuation *Proc. MEMS'2000 (Miyazaki)* pp 715–20

[8] Young W C and Budynas R G 2002 *Roark's Formulas for Stress and Strain* 7th edn (New York: McGraw-Hill)

[9] Xiao Z, Wu X T, Peng W and Farmer K R 2001 An angle-based design approach for rectangular electrostatic torsion actuators *J. Microelectromech. Syst.* **10** 561–8

[10] Debray A, Ludwig A, Bourouina T, Asaoka A, Tiercelin N, Reyne G, Oki T, Quandt E, Muro H and Fujita H 2004 Application of a multilayered magnetostrictive film to a micromachined 2-D optical scanner *J. Microelectromech. Syst.* **13** 264–71

[11] Chabot M D and Markert J T 1999 Microfabrication of single-crystal silicon multiple torsional oscillators *Proc. SPIE* **3875** 104–12

[12] Huang L S, Lee S S, Motamedi M E, Wu M C and Kim C J 1998 Optical coupling analysis and vibration characterization for packaging of 2 × 2 MEMS vertical torsion mirror switches *Proc. SPIE* **3513** 135–43

[13] Urey H 2002 Torsional MEMS scanner design for high-resolution display systems *Proc. SPIE* **4773** 27–37

[14] Meirovitch L 1967 *Analytical Methods in Vibrations* (New York: Macmillan)

[15] Weaver W, Timoshenko S P and Young D H 1990 *Vibration Problems in Engineering* (New York: Wiley)

[16] Timoshenko S P and Goodier J N 1951 *Theory of Elasticity* (New York: McGraw-Hill)

[17] Love A E H 1944 *A Treatise on the Mathematical Theory of Elasticity* (New York: Dover)

[18] Schiltges G, Gsell D and Dual J 1998 Torsional tests on microstructures: two methods to determine shear-moduli *Microsyst. Technol.* **5** 22

[19] Boresi A P and Chong K P 2000 *Elasticity in Engineering Mechanics* (New York: Wiley)

[20] Juneau T N 1998 Micromachined dual input axis rate gyroscope *PhD dissertation* University of California, Berkeley, CA

[21] Davis W O, O'Reilly O M and Pisano A P 2004 On the nonlinear dynamics of tether suspensions for MEMS *J. Vib. Acoust.* **126** 326–31

[22] Han S M, Benaroya H and Wei T 1999 Dynamics of transversely vibrating beams using four engineering theories *J. Sound Vib.* **225** 936–7

[23] Reddy J N, Wang C M and Lee K H 1997 Relationships between bending solutions of classical and shear deformation beam theories *Int. J. Solids Struct.* **34** 3373–84

[24] Wang C M 1995 Timoshenko beam-bending solutions in terms of Euler–Bernoulli solutions *J. Eng. Mech.* **121** 763–5

[25] Kaneko T 1975 On Timoshenko's correction for shear in vibrating beams *J. Phys. D: Appl. Phys.* **8** 1927–36

[26] Hutchinson J R 2001 Shear coefficients for Timoshenko beam theory *J. Appl. Mech.* **68** 87–92

[27] Puchegger S, Loidl D, Kromp K and Peterlik H 2003 Hutchinson's shear coefficient for anisotropic beams *J. Sound Vib.* **266** 207–16

[28] Cowper G R 1966 The shear coefficient in Timoshenko's beam theory *ASME J. Appl. Mech.* **33** 335–40

[29] Davis W O and Pisano A P 1998 On the vibration of a MEMS gyroscope *Proc. 1st Int.Conf. on the Modeling and Simulation of Microsystems, Semiconductors, Sensors, and Actuators (MSM'98) (Santa Clara, CA 6–8 April, 1998)* pp 557–62

[30] Wortman J J and Evans R A 1965 Young's modulus, shear modulus, and Poisson's ratio in silicon and germanium *J. Appl. Phys.* **36** 153–6

[31] Cazzani A and Rovati M 2003 Extrema of Young's modulus for cubic and transversely isotropic solids *Int. J. Solids Struct.* **40** 1713–44

[32] Sokolnikoff I S 1956 *Mathematical Theory of Elasticity* 2nd edn (New York: McGraw-Hill)

[33] Senturia S D 2001 *Microsystem Design* (Boston: Kluwer) pp 192–3

[34] Schenk H, Dürr P, Kunze D, Lakner H and Kück H 2001 A resonantly excited 2D micro-scanning-mirror with large deflection *Sensors Actuators* A **89** 104–11

[35] Ataman C, Kaya O and Urey H 2004 Analysis of parametric resonances in comb-driven microscanners *Proc. SPIE* **5455** 128–36